Triangular Shaped QMSIW Cavity Back Slot Antenna for Tri-Band Operation

Dokuparthi Jagadeesh[*] **and Alapati Sudhakar**

Abstract—In this paper, a triangle-shaped Quarter Mode Substrate Integrated Waveguide (QMSIW) cavity back slot antenna is developed using TE_{110}, TE_{220}, and $TE_{310,130}$ modes for tri-band operation. The QMSIW is obtained from the quadrant part of a square SIW (Substrate Integrated Waveguide) structure. The electric field distributions of resonant modes are studied for the Full Mode SIW, Half Mode SIW, and Quarter Mode SIW cavities through HFSS simulation tool. The generation of the hybrid mode $TE_{310,130}$ mode is clearly explained with the simulation tool. A rectangular slot is engraved on top layer of the structure along the perfect electric wall, to radiate the EM (Electro Magnetic) wave towards positive Z-direction. Further, a metallized via has been inserted to bring reflection coefficient below -10 dB at the three resonant modes. The developed antenna achieves resonance at 5.2 GHz, 9.88 GHz, and 10.6 GHz frequencies with peak gains of 9 dB, 6.2 dB, and 7.9 dB, respectively. The antenna is designed on a single layer thin substrate which reduces the fabrication complexity.

1. INTRODUCTION

There has been a tremendous development in the field of present wireless communication that requires compact size and high gain antennas. SIW technology has the ability to miniaturize SIW cavity back antennas by cutting along a perfect magnetic wall. Moreover, SIWs have high power handling capability, high Q-factor, and flexibility to integrate with planar circuits. A line fed QMSIW antenna is developed in [1]. Here, initially a square cavity resonator is designed, and later, it is cut along a magnetic wall to obtain Half-Mode SIW. The HMSIW is again cut along another magnetic wall which is normal to the first one to accomplish QMSIW. The resulting structure is in triangular shape which contains a perfect electric wall at one side, i.e., series of metallized vias and two magnetic walls at other two sides. It is shown that the field distribution of the quadrant sector is the same as that of a square cavity resonator. Also, it is demonstrated that the two magnetic walls serve as a radiator coupling electromagnetic energy from cavity to the free space. A line fed QMSIW antenna is presented [2] to achieve dual-band response in S-band range. Here, top of the layer is loaded by Minkowski fractal geometry for further size reduction. A QMSIW slot antenna operating in UHF (Ultra High Frequency) band is presented [3] in which two perpendicular rectangular slits are loaded on the uppermost layer. A QMSIW based antenna for WLAN (Wireless Local Area Network) applications is presented [4] in which top of the layer is loaded with a Sierpinski fractal structure while Complementary Split Ring Resonator (CSRR) is engraved on the ground layer. The frequency tuning is observed when the CSRR structure is rotated from 0° to 315°. Two HMSIW cavity back slot antennas for WLAN applications are developed [5]. Here, one of the antenna's Perfect Electric Wall (PEC) is designed by single series of vias. The other is designed by two series of vias. It is proved that the cavity back antenna designed by two series of vias has achieved improvement in radiation characteristics. A circular QMSIW cavity backed slot antenna for ISM (Industrial, Scientific and Medical) band applications is presented [6] in

which TM_{210} and TM_{020} modes are brought closer by introducing a rectangular slot on the top layer. This phenomenon increases the bandwidth of the antenna. The bandwidth is further improved by tilting the slot. A compact multi-layer SIW cavity back antenna [7] is developed by placing a QMSIW cavity over an FMSIW cavity. The FMSIW and QMSIW cavities are responsible for higher and lower bands, respectively. A compact HMSIW antenna loaded by two U-shaped strips [8] is developed to achieve tri-band resonance. The HMSIW structure excited in TE_{110} mode achieves resonance at lower band while the two U-shaped strips are responsible for achieving two additional resonances. The ring slot loaded circular SIW cavity back slot antenna [9] is developed to achieve tri-band response. By optimizing feed location, the antenna is excited in TM_{110}, TM_{020}, and TM_{120} modes. The three resonant frequencies of the three modes are independently tuned by changing geometrical parameters of the antenna. An antenna developed on a leather substrate [10] has achieved resonance at three different frequencies. It is constructed based on HMSIW technique to get miniaturization. To achieve further miniaturization, the structure is loaded by two rectangular slits. However, it suffers from low gain as the substrate has high loss tangent.

In this article, a tri-band cavity backed antenna based on QMSIW is proposed. It is a triangle-shaped, miniaturized antenna which operates at 5.2 GHz, 9.88 GHz, and 10.6 GHz frequencies. A non-resonance rectangular slot is engraved on top of the QMSIW structure to obtain peak gain at boresight direction. Further, the structure is loaded by metallized vias to optimize the reflection coefficient at three operating bands. The resultant structure achieves more than 6 dB gain along with a size reduction up to 75% compared with conventional SIW cavity back antenna.

2. ANTENNA STRUCTURE

The geometrical shape and dimensions of the tri-band QMSIW antenna are exhibited in Fig. 1 and Table 1, respectively. An RT Duroid 5880 substrate ($\varepsilon_r = 2.2$) is selected to design the antenna as it has low loss tangent factor (0.0009). Fig. 1 shows that the antenna shape appears like a right angled triangle. However, two of three corners of the triangle are flattened. Top and bottom of the substrate
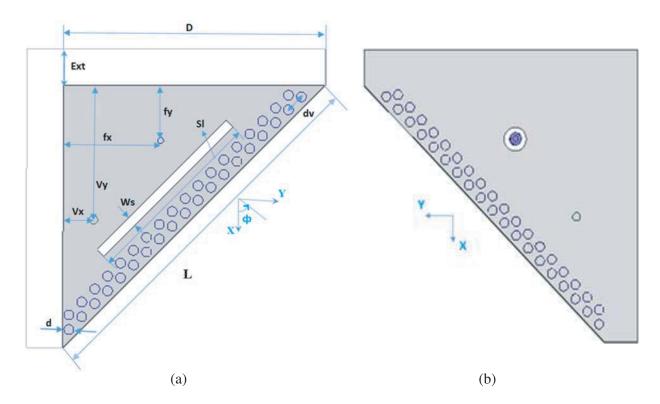

Figure 1. Structure of proposed tri-band antenna. (a) Front view. (b) Rear view.

Table 1. Parameters of the proposed antenna.

Parameter	Value (mm)	Parameter	Value (mm)
D	21.5	d	0.8
Ext	3	dv	1.5
Sl	15	fx	4.5
Ws	0.8	fy	8
Vx	11	Vy	2.5
L	30.4		

are coated by a thin copper layer. However, top of the substrate is not completely coated by a thin copper layer in the two orthogonal sides. Some portion of these two sides is left open with a width of '3 mm' for radiation. One side of the triangle is filled with two rows of vias which behave like a perfect electric wall that prevents leakage of EM wave energy. Thus, the structure in this case is said to be QMSIW cavity. A rectangular slot is engraved on top of the layer near the two series of vias. The resulting structure is excited using the probe feed method whose location is optimized using HFSS tool.

3. DESIGN PROCESS OF THE ANTENNA

There are two steps in the design of the proposed antenna. First one is the realization of QMSIW cavity, and the second is making slot and inserting metallized vias at appropriate positions to achieve resonance at multiple frequencies. Initially, a square FMSIW cavity resonator is designed using Eqs. (1)–(2).

$$f_{mnp} = \frac{1}{2\sqrt{\mu_0 \varepsilon_0 \varepsilon_r}} \sqrt{\left(\frac{m}{L_{eff}}\right)^2 + \left(\frac{n}{L_{eff}}\right)^2 + \left(\frac{p}{h}\right)^2} \tag{1}$$

$$L_{eff} = L - 1.08 \frac{d^2}{d_v} + 0.1 \frac{d^2}{L} \tag{2}$$

where L and h represent length and height of the FMSIW cavity; d and dv are the diameter of each via and spacing between the adjacent vias, respectively. Here, m, n, and p are integers which show the number of field variations along three orthogonal sides.

Since it is a square cavity, several degenerating modes can be excited in the structure. A hybrid mode $TE_{310,130}$ is formed by merging TE_{310} and TE_{130} modes. TE_{110}, TE_{220}, and $TE_{310,130}$ modes have been chosen to develop a tri-band antenna. The simulated resonant frequencies of the square SIW cavity for TE_{110}, TE_{220}, and $TE_{310,130}$ modes are 5.5 GHz, 10.7 GHz, and 11.8 GHz. The magnitude of electric field variations over the structure in the modes are exhibited in Fig. 2. It explicates that the three modes are symmetric about the Y-axis. Hence, the designed square cavity is bisected along the magnetic wall which is parallel to Y-axis to achieve 50% reduction in size.

The developed HMSIW preserves field distributions of the three modes and exhibits slight changes in resonant frequencies due to dielectric aperture at the magnetic wall. The resonant frequencies of the HMSIW reach 5.6 GHz, 10.9 GHz, and 11.9 GHz at TE_{110}, TE_{220}, and $TE_{310,130}$ modes, respectively. The magnitudes of electric field variation over the cavity surface are exhibited in Fig. 3 which is symmetric about X-axis.

The developed HMSIW can again be cut along magnetic wall to achieve 75% reduction in size. The resultant structure is named as QMSIW cavity which preserves the three resonant modes with small change in resonant frequencies. The resonant frequencies of the QMSIW cavity for the above modes reach 5.4 GHz, 10.5 GHz, and 11.7 GHz. The magnitudes of electric field variation over QMSIW cavity are shown in Fig. 4.

The dielectric apertures provided at two magnetic walls affect the resonant frequencies of the cavity. The two dielectric apertures are provided at the top of the miniaturized QMSIW structure by extending ground plane. This enables the structure to radiate EM wave towards positive Z-direction. The radiation from the two edges deviates the peak gain from the boresight direction. Hence, a rectangular
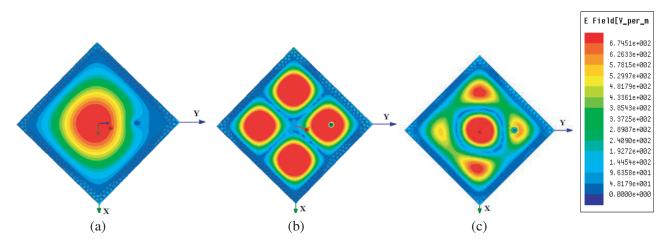
Figure 2. E-field distributions of FMSIW structure in (a) TE_{110} mode: 5.5 GHz, (b) TE_{220} mode: 10.7 GHz, (c) $TE_{310, 130}$ mode: 11.8 GHz.
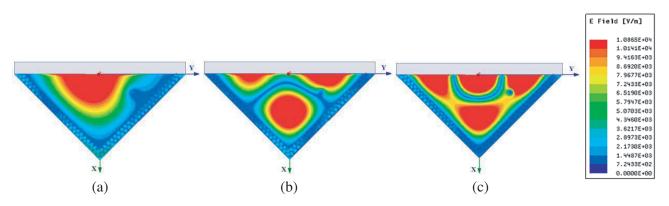

Figure 3. E-field distributions of HMSIW structure in (a) TE_{110} mode: 5.6 GHz, (b) TE_{220} mode: 10.9 GHz, (c) $TE_{310,130}$ mode: 11.9 GHz.
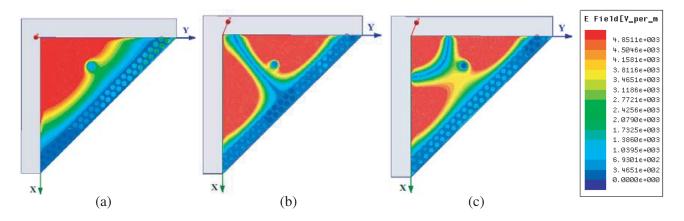

Figure 4. E-field distributions of the QMSIW structure at (a) 5.4 GHz: TE_{110} mode, (b) 10.5 GHz: TE_{220} mode, (c) 11.7 GHz: $TE_{310,130}$ mode.

slot is engraved the on top layer near the two series of metallized vias. This enables the structure to radiate EM wave from all the three sides of the triangular structure which leads to achieving a perfect unidirectional radiation pattern. The impedance matching of the structure is further improved by inserting a metallized via. By varying the position and diameter of the metallized via, the impedance

matching is achieved at the three bands.

The rotation of the E-field distribution shown in Fig. 5 explicates that the proposed antenna produces Right Hand Circularly Polarized (RHCP) wave. The variation of E-field magnitude over the top surface can be observed in Fig. 5 at different phase angles. It shows that the magnitude of the E-field is rotated in anticlockwise direction when the phase varies from 0° to 180°. The distribution has two peak magnitudes as it is plotted at TE$_{220}$ mode. An arrow is drawn at the middle of the two peaks and is used to trace the rotation of the E-field distribution with respect to the phase. The arrow is at 100°, 140°, 170°, 225°, 280°, and 315° when $\Phi = 0°$, 40°, 80°, 120°, 160°, and 180°. This clearly indicates that the E-field rotates in anticlockwise direction, and the antenna radiates towards top direction. The direction EM wave propagation can be represented with right-hand thumb, and the remaining four fingers match with E-field direction (anti-clockwise direction). Hence, the radiated EM wave is said to be RHCP wave. Left Hand Circularly Polarized (LHCP) wave is also observed when the feed position is mirrored along $\Phi = 45°$ axis.
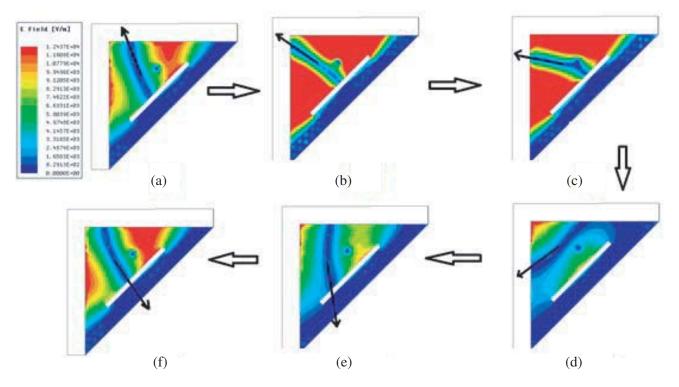

Figure 5. E-field distribution at 9.88 GHz for different phase angles, (a) $\Phi = 0°$, (b) $\Phi = 40°$, (c) $\Phi = 80°$, (d) $\Phi = 120°$, (e) $\Phi = 160°$, (f) $\Phi = 180°$.

The generation of the hybrid mode is illustrated in Fig. 6. Figs. 6(a) and (b) show the TE$_{130}$ and TE$_{310}$ modes respectively in which the total area is classified into three regions. Each region indicates one half mode. As TE$_{130}$ and TE$_{310}$ modes occur simultaneously, the resultant field distribution will be the sum of the two field distributions. A total of nine regions are formed when Figs. 6(a) and (b) are superimposed. The resultant field distribution shown in Fig. 6(c) consists of nine regions. The red colour in the figure indicates positive field while negative field is indicated by orange colour. There are two negative fields combined in regions 1, 3, 7, and 9. The resultant field will be more negative in these regions. In regions 2, 4, 6, and 8, there is a combination of one positive field and one negative field which yield cancellation of the fields. The field in region 5 is the combination of two positive fields which results in a more positive field. The resultant fields in the regions are shown in Fig. 6(d). This analysis has been verified by simulating E-field vector of the hybrid mode which is shown in Fig. 6(e). Here, the E-field at the centre is in upward direction which indicates the positive field while the field is in downward direction at the corners of the structure that indicates negative field.
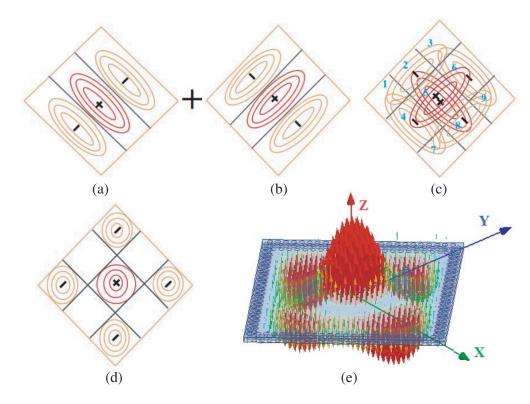
Figure 6. Hybrid mode formation: E-field distribution of (a) TE_{130} mode, (b) TE_{310} mode, (c) superimposing of TE_{130} and TE_{310} modes (hybrid mode), (d) resultant filed distribution, (e) simulated E-field vector of hybrid mode $TE_{130,310}$.

The inserted metallized via allows the current from bottom to the top metal layer through the substrate. It adds parallel inductance to the structure. The resultant inductance of the structure is the parallel combination of inductance formed by metallized via and cavity inductance. Consequently, the overall inductance of the structure is reduced. Further, the resonant frequencies of the structure are shifted up as there is an inverse relation between inductance and resonant frequency of the SIW cavity. The change in resonant frequencies of the structure before and after placing the metallized via are shown in Fig. 7(a). It also shows that reduction in overall inductance of the structure improves the impedance matching at the three desired bands.

The QMSIW structure loaded by slot and metallized via resonates at three frequencies. Parametric analysis has been performed to observe the variation of reflection coefficient with the change in slot length. It is observed from Fig. 7(b) that the reflection coefficient at band1 has no effect with changes in slot length while upper bands are effected significantly with changes in slot length. The resonant frequencies of the higher bands decrease with increasing slot length. The capacitance introduced by the longer slot is higher than the shorter slot as the area of cross-section is large for longer slot. Also, the capacitance is directly proportional to the area of cross-section. Thus, the longer slot introduces large capacitance which causes the decrease of the resonant frequencies at higher bands of the proposed antenna.

From Fig. 7(b), it is evident that the reflection coefficient has arrived below $-20\,dB$ at higher bands when slot length is 15 mm. The simulated reflection coefficients at this slot length are $-33\,dB$, $-26\,dB$, and $-23\,dB$ at the centre frequencies of 5.2 GHz, 9.77 GHz, and 10.52 GHz, respectively.

4. EXPERIMENTAL RESULTS AND DISCUSSION

A photograph of the fabricated antenna is exhibited in Fig. 8. The $|S_{11}|$ in dB of the resulted antenna has been measured using Anritsu VNA (Vector Network Analyzer). The measured $|S_{11}|$ shown in
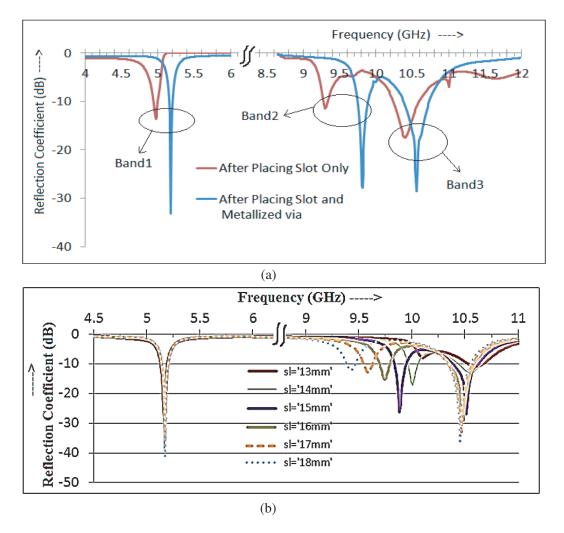
(a)

(b)

Figure 7. Reflection coefficient, (a) after placing slot and metallized via, (b) for variation of slot length.

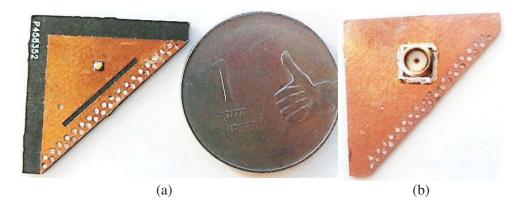(a)   (b)

Figure 8. Photograph of the fabricated antenna. (a) Top view. (b) Bottom view.

Fig. 9 explicates that the antenna resonates at three different frequencies. The experimental fractional impedance bandwidths at three operating bands are 1%, 1.3%, and 3.7% at the centre frequencies of 5.2 GHz (1st band), 9.88 GHz (2nd band), and 10.6 GHz (3rd band), respectively. The secondary axis (Right side) of the figure designates the gain and axial ratios at boresight directions. The measured
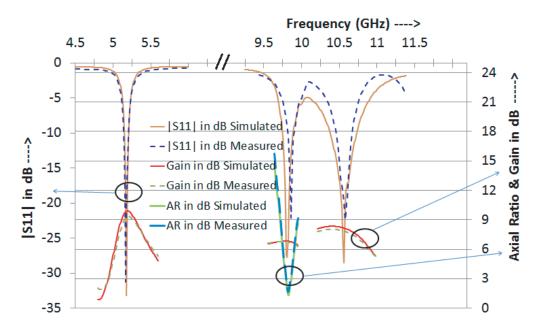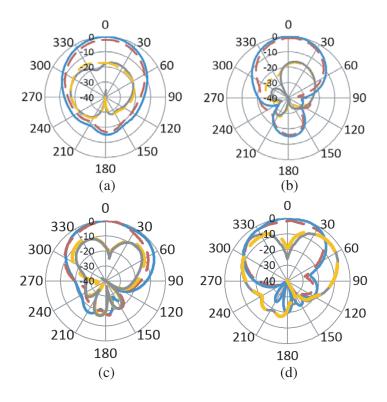
Figure 9. Reflection coefficient, gain and axial ratio of the proposed tri-band antenna.

gains reach 9 dB, 6.2 dB, and 7.9 dB at the mid frequencies of 1st, 2nd, and 3rd bands, respectively. The radiation of circularly polarized wave at the 2nd band is ensured by measuring axial ratio (AR) at boresight direction. The AR in dB value at the 2nd band centre frequency is 1.34 dB. There exist a small deviation between the simulated and experimental results due to losses offered by the SMA connectors and conductors which were not included in the simulation.

The normalized radiation patterns of the proposed antenna at the three operating bands are exhibited in Figs. 10(a)–(f). It is clearly illustrated that the proposed antenna accomplishes
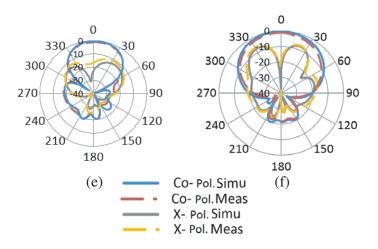

(a)

(b)

(c)

(d)

Figure 10. Normalized radiation patterns at (a) 5.2 GHz: E-plane, (b) 5.2 GHz: H-plane, (c) 9.88 GHz: $\Phi = 45°$ plane, (d) 9.88 GHz: $\Phi = 135°$ plane, (e) 10.6 GHz: E-plane, (f) 10.6 GHz: H-plane.

unidirectional radiation pattern as its Front-To-Back Ratio (FTBR) crosses 18 dB in the three operating bands. Figs. 10(a) and (b) are the patterns of the first band centre frequency at two perpendicular planes, E-plane ($\Phi = 45°$) and H-plane ($\Phi = 135°$), respectively. Achieved angular 3-dB beamwidth here is about $70°$. The difference between peak co-polarization and cross-polarization levels (CPL) exceed 17 dB in the boresight direction.

Table 2. Comparison of proposed antenna performance with Ref. antennas.

Ref.	Centre Frequencies (GHz)	No. of bands	Antenna Size	ε_r	Fraction Impedance Bandwidth (%)	height (mm)	Peak Gain (dB)	Operating Band(s)
[11]	7.39, 9.43, 14.79	3	$0.5664\lambda_0^2$	2.2	1.35, 2.33, 2.23	0.8	3.2, 4.9, 4.7	C-, X- and Ku-bands
[12]	4.01, 5.81, 6.55	3	$0.9957\lambda_0^2$	2.2	2.4, 2.2, 1.6	1.6	7.75, 8.35, 7.32	C-band
[13]	4.66, 8.3	2	$0.8649\lambda_0^2$	2.7	NM NM	0.8	4.5, 5	C- and X-bands
[14]	4.3, 9.45	2	$0.7396\lambda_0^2$	2.7	NM NM	0.8	3.53, 6.71	C- and X-bands
[15]	8.68, 10.8	2	NM	2.2	0.92, 1.57	0.8	7.7, 9	X-band
[16]	8.5, 10.6	2	$0.3901\lambda_0^2$	2.2	2.75, 3.42	0.8	7.5, 6	X-band
This work	5.2, 9.88, 10.6	3	$0.1109\lambda_0^2$	2.2	1, 1.3, 3.7	0.8	9, 6.2, 7.9	C- and X-bands

NM — Not Mentioned

Figures 10(c) and (d) depict patterns of the 2nd band centre frequency at two perpendicular planes ($\phi = 45°$ and $\phi = 135°$). It is observed that the RHCP wave is generated with peak magnitude in the boresight direction. The peak CPL within the 3-dB angular beamwidth is lower than -18 dB in the two perpendicular planes. Figs. 10(e) and (f) represent the E- and H-plane radiation patterns at the third band centre frequency corresponding to $\Phi = 45°$ and $\Phi = 135°$, respectively. It is evident that the measured peak CPL is 17 dB less than desired polar level in the boresight direction.

The proposed tri-band antenna performance is assessed through comparison table. The term λ_0 in Table 2 indicates the wavelength of the lower operating frequency. The proposed antenna exhibits high compactness and tri-band response along with significant improvement in gain compared with ref. antennas [11–16].

5. CONCLUSION

A triangle-shaped QMSIW cavity back slot antenna is presented in this paper. It achieves tri-band resonance when it is excited by TE_{110}, TE_{220}, and $TE_{310,130}$ modes. A rectangular slot etched near the PEC wall helps to accomplish a perfect unidirectional radiation pattern. Further, the impedance matching at three operating bands is improved by inserting a metallized via. The resulting antenna accomplishes a size reduction up to 75% compared with conventional SIW cavity back antenna. The antenna is developed on a thin substrate which makes the device light weight. Hence, it is well suitable for compact devices. The antenna operates at 5.2 GHz, 9.88 GHz, and 10.6 GHz frequencies with significant gain. Hence, the proposed antenna is well preferred for WLAN and X-band applications.

REFERENCES

1. Jin, C., R. Li, A. Alphones, and X. Bao, "Quarter-mode substrate integrated waveguide and its application to antennas design," *IEEE Transactions on Antennas and Propagation*, Vol. 61, No. 6, 2921–2928, 2013.
2. Fu, Z., T. Zhang, Y. Lan, T. Wu, W. Huang, and L. He, "Dual-frequency miniaturized substrate integrated waveguide quarter-mode cavity-backed antenna based on Minkowski fractal gap with orthogonal polarization radiation characteristics," *International Journal of Antennas and Propagation*, 2019.
3. Casula, G. A., "A quarter mode SIW antenna for short range applications," *2nd URSI AT-RASC*, Gran Canaria, 2018.
4. Choudhury, S. and A. Mohan, "Miniaturized Sierpinski fractal loaded QMSIW antenna with CSRR in ground plane for WLAN applications," *Microw. Opt. Technol. Lett.*, Vol. 59, No. 6, 1291–1295, 2017.
5. Anand, S. and D. Rokhini, "A double line SIW cavity backed antenna for WLAN applications," *Int. J. RF Microw. Comput. Aided Eng.*, Vol. 29, No. 11, e21861, 2019.
6. Chaturvedi, D. and S. Raghavan, "A quarter-mode SIW based antenna for ISM band application," *IEEE International Conference on Antenna Innovations & Modern Technologies for Ground, Aircraft and Satellite Applications (iAIM)*, 2017.
7. Yue, T. and D. H. Werner, "A compact dual-band antenna based on SIW technology," *IEEE International Symposium on Antennas and Propagation & USNC/URSI National Radio Science Meeting*, 2018.
8. Yang, X., L. Ge, Y. Ji, X. Zeng, and K. M. Luk, "Design of low-profile multi-band half-mode substrate-integrated waveguide antennas," *IEEE Transactions on Antennas and Propagation*, Vol. 67, No. 10, 6639–6644, 2019.
9. Guan, D., Z. Qian, W. Cao, L. Ji, and Y. Zhang, "Compact SIW annular ring slot antenna with multiband multimode characteristics," *IEEE Transactions on Antennas and Propagation*, Vol. 63, No. 12, 5918–5922, 2015.
10. Mandal, B. and S. K. Parui, "Wearable tri-band SIW based antenna on leather substrate," *Electronics Letters*, Vol. 51, No. 20, 1563–1564, 2015.

11. Soumava, M. and B. Animesh, "Computer aided equivalent circuit model of SIW cavity backed triple band slot antenna," *International Journal of RF and Microwave Computer-Aided Engineering*, Vol. 27, No. 2, e21060, 2016.

12. Alhalboosi, H. A., S. Kurnaz, and A. M. Shantaf, "Design of double H-slot microstrip patch triple-band for C-band," *International Congress on Human-Computer Interaction, Optimization and Robotic Applications (HORA)*, 2020.

13. Banerjee, S. and M. Gangopadhyaya, "A compact dual-band half-mode SIW based semicircular antenna," *IEEE 7th Annual Ubiquitous Computing, Electronics & Mobile Communication Conference (UEMCON)*, 2016.

14. Banerjee, S., S. Chatterjee, S. D. Mazumdar, M. Gangopadhyaya, and B. Rana, "Multi-slot loaded dual band compact half-mode SIW triangular antenna," *Advances in Optical Science and Engineering*, 441–448, 2017.

15. Mukherjee, S., K. V. Srivastava, and A. Biswas, "Implementation of dual-frequency longitudinal slot array antenna on substrate integrated waveguide at X-band," *Proc. of Eur. Microw. Conf. (EuMC)*, 195–198, 2013.

16. Jagadeesh, D. and S. Alapati, "Dual band half mode SIW semi circular cavity back slot antenna," *Progress In Electromagnetics Research Letters*, Vol. 87, 7–14, 2019.